2RT PAPER SUMMARY

Retinal Damage Profiles and Neuronal Effects of Laser Treatment: Comparison of a Conventional Photocoagulator and a Novel 3-Nanosecond Pulse Laser.

Aim: Evaluate retinal cell and neurons in response to application of conventional thermal laser and new 2RT nanopulse laser and to determine if new nanopulse laser can specifically ablate RPE cells without collateral damage to other retinal cells. Laboratory animal study on rats. 2RT laser was applied at two distinct energy settings: above and below visible effect threshold.

Summary Outcome: Treatment with conventional thermal laser caused the rapid appearance of lesions that were associated with ablated RPE, induction of both delayed and instant photoreceptor death and widespread edema. Use of the 2RT laser at either the high or low setting led to RPE loss with sparing of Bruch's membrane. 2RT applied at energy levels clinical significant for treatment of DME patients causes an RPE lesion that is entirely specific to these cells and leaves an intact basement membrane which is largely repaired in 7 days. 2RT has wider potential applications as it does not cause the same degree of collateral tissue damage when kept at subvisible energy levels as with conventional thermal laser.

Retinal Damage Profiles and Neuronal Effects of Laser Treatment: Comparison of a Conventional Photocoagulator and a Novel 3-Nanosecond Pulse Laser

John P. M. Wood,[1–3] *O'Sam Shibeeb,*[1,2] *Malcolm Plunkett,*[4] *Robert J. Casson,*[1,2] *and Glyn Chidlow*[1–3]

Purpose. To determine detailed effects to retinal cells and, in particular, neurons following laser photocoagulation using a conventional 532 nm Nd:YAG continuous wave (CW) laser. Furthermore, to determine whether a novel 3 ns pulse laser (retinal regeneration therapy; 2RT) could specifically ablate retinal pigment epithelium (RPE) cells without causing collateral damage to other retinal cells.

Methods. Adult Dark Agouti (DA) rats were separated into four groups: control, CW laser (12.7 J/cm^2/pulse, 100 ms pulse duration), or 3 ns pulse 2RT laser at one of two energy settings ("High," 2RT-H, 163 mJ/cm^2/pulse; "Low," 2RT-L, 109 mJ/cm^2/pulse). Animals were treated and killed after 6 hours to 7 days, and retina/RPE was analyzed by histologic assessment, Western blot, polymerase chain reaction, and immunohistochemistry.

Results. Both lasers caused focal loss of RPE cells with no destruction of Bruch's membrane; RPE cells were present at lesion sites again within 7 days of treatments. CW and 2RT-H treatments caused extensive and moderate damage, respectively, to the outer retina. There were no obvious effects to horizontal, amacrine, or ganglion cells, as defined by immunolabeling, but an activation of PKCα within bipolar cells was noted. There was little discernible damage to any cells other than the RPE with the 2RT-L treatment.

Conclusions. Conventional laser photocoagulation caused death of RPE cells with associated widespread damage to the outer retina but little influence on the inner retina. The novel 3 ns 2RT laser, however, was able to selectively kill RPE cells without causing collateral damage to photoreceptors. Potential benefits of this laser for clinical treatment of diabetic macular edema are discussed. (*Invest Ophthalmol Vis Sci.* 2013; 54:2305–2318) DOI:10.1167/iovs.12-11203

Since publication of the Early Treatment Diabetic Retinopathy Study (ETDRS), retinal laser photocoagulation has represented the routine tool for clinical management of diabetic macular edema (DME).[1–5] In recent years, however, treatment of DME has been revolutionized by the advent of intravitreal, anti-vascular endothelial growth factor (anti-VEGF) therapy. Nevertheless, since the long-term outcomes of this strategy are as yet unclear, many clinicians still believe that retinal lasers have a continuing role to play in the management of DME and indeed other retinal conditions.[6–8] This treatment is traditionally carried out with continuous wave lasers having wavelengths in the green region of the visible spectrum (usually 514 or 532 nm).[3–5] Laser irradiation is converted to heat energy at the melanosomes of the retinal pigment epithelium (RPE) and choroid.[2] The mechanism by which photocoagulation reduces DME remains speculative, although suggestions have included the reduction in capillary permeability or the increase in active transport of fluid from retina to blood.[9,10] Furthermore, photocoagulation can cause collateral damage to the overlying sensory retina, subretinal fibrosis, and enlargement of burns with time, with potentially devastating visual results.[9,11,12]

More recent research has focused on reducing the absorbed laser energy such that it can be specifically confined to the RPE and thus collateral retinal damage reduced or avoided.[13] This can be accomplished, for example, by reducing the power setting, increasing the laser wavelength, or using either a shorter-duration pulse or noncontinuous wave micropulses.[14–18] To this end, we have recently described a novel laser that shares characteristic features with conventional 532 nm wavelength lasers but has a nanosecond-range pulse duration.[19] We have shown in vitro that this laser, the retinal regeneration therapy (2RT) system, specifically ablates RPE cells and causes minimal collateral damage to photoreceptors at clinically relevant energy settings.[19] Furthermore, the 2RT laser has already been tested for treatment of DME patients in the clinic and shown to have an effect on retinal thickness reduction similar to that with the conventional continuous wave (CW) laser.[20,21]

Although retinal-sparing laser regimens, including the use of short-pulse nanosecond lasers, are proving to be just as efficacious as the modified ETDRS procedure in providing therapeutic benefit to DME patients,[16,20,22] it is crucial to the understanding of the ameliorative mechanism of retinal laser treatment in general that detailed cellular effects to the retina be elucidated. In particular, it is essential to understand whether neurons are adversely affected following therapeutic

From the [1]Ophthalmic Research Laboratories, South Australian Institute of Ophthalmology, Hanson Institute Centre for Neurological Diseases, Adelaide, South Australia, Australia; the [2]Department of Ophthalmology and Visual Sciences, University of Adelaide, Adelaide, South Australia, Australia; and [4]Ellex R&D Pty. Ltd., Adelaide, South Australia, Australia.

[3]These authors contributed equally to the work presented here and should therefore be regarded as equivalent authors.

Supported in part by Ellex R&D Pty. Ltd. and the Australian Government Department of Industry Tourism and Resources (AusIndustry); financial assistance from the University of Adelaide (JPMW, RJC).

Submitted for publication October 25, 2012; revised January 8 and February 6, 2013; accepted February 18, 2013.

Disclosure: **J.P.M. Wood**, None; **O'S. Shibeeb**, None; **M. Plunkett**, Ellex R&D Pty. Ltd. (E); **R.J. Casson**, None; **G. Chidlow**, None

Corresponding author: John P. M. Wood, Ophthalmic Research Laboratories, Hanson Centre for Neurological Diseases, Frome Road, Adelaide, SA 5000, Australia; john.wood@health.sa.gov.au.

lasing. To date, histologic damage to the retina, in particular to photoreceptors, after conventional laser photocoagulation treatment has been well documented[15,23–31]; but while it is generally accepted that damage does not extend past the photoreceptors into the inner retina, detrimental effects have been observed.[27,32–36] These data suggest that the inner neural retina can be affected in some manner by standard laser photocoagulation.

The first aim of the present study, therefore, was to treat rat eyes with a conventional Nd:YAG CW laser at a clinically relevant energy setting, both to prove that an ablation of focal target RPE cells occurs and to determine the full detrimental effect to distinct classes of retinal neurons including photoreceptors. The second aim was to repeat these tests using the nanosecond pulse 2RT laser in order to determine whether this system was able to cause an effect on the RPE similar to that with the CW laser but without the same degree of collateral damage to the retina, as suggested from in vitro studies.[19]

Materials and Methods

Lasers

Two lasers were used for treatment of animals: Both were frequency-doubled Nd:YAG lasers with 532 nm wavelengths and were provided by Ellex R&D Pty. Ltd. (Adelaide, SA, Australia). A 5.4 mm fundus laser contact lens (Ocular Instruments, Bellevue, WA) was used to focus the light beam onto the retina in each case. The first laser had a single 3 ns pulse duration with a 380 μm diameter spot size in air and a 285 μm diameter spot size on the rat retina, and a fine speckle beam profile (the nanosecond laser; 2RT). The 2RT laser was used at two different energy settings (see Table 1). The first was defined as the setting at which the operator was able to discern a clearly visual and consistent effect on the eye at the time of laser application (i.e., *suprathreshold*); this was identified as a subtle blanching and was defined as the "high" energy setting (2RT-H; 163 mJ/cm^2/pulse). A similar energy setting was used in the 2RT clinical trials to range find for each patient.[20,21] The second energy setting was equivalent to that being used in 2RT clinical trials for DME and equated to exactly two-thirds of the 2RT-H energy level (i.e., *subthreshold*; see Table 1); this was defined as the "low" energy setting (2RT-L; 109 mJ/cm^2/pulse). Previous in vitro experiments had established that this lower energy setting was within the therapeutic range of the laser.[19] The second laser used in the study was a CW laser, with a 400 μm diameter spot, a flat top beam profile, and a total beam exposure duration of 100 ms. This laser was used at the 90 mW setting, which equates to a radiant exposure level of 12.7 J/cm^2/pulse and produces light laser burns, defined as blanching of the fundus pigmentation (but without candid whitening) and devoid of adjacent edema or subretinal or retinal hemorrhage.

Treatment of Animals

This study was approved by the Animal Ethics Committees of SA Pathology and the University of Adelaide. The study conformed to the Australian Code of Practice for the Care and Use of Animals for Scientific Purposes (2004) and to the ARVO Statement for the Use of Animals in Ophthalmic and Vision Research. Adult Dark Agouti rats (approximately 150 g) were housed in a temperature- and humidity-controlled room with a 12-hour light, 12-hour dark cycle and were provided with food and water ad libitum.

Prior to induction of laser treatment, rats were anesthetized with an intraperitoneal injection of a mixture of 100 mg/kg ketamine and 10 mg/kg xylazine. When general anesthesia had been obtained, the pupils were dilated by topical application of tropicamide, allowing visualization of the optimum area of retina through the eye. Animals were then placed on a custom-designed platform attached to the slit-lamp laser delivery system. Rats were randomly assigned to one of three treatment groups: CW, 2RT-H, or 2RT-L. For animals that were subsequently used for Western immunoblotting or RT-PCR, approximately 100 laser spots were applied randomly to each retina around the optic nerve head, taking care to avoid the macula region and major blood vessels; all spots were applied in the posterior hemisphere of the eye. For animals that were subsequently used for histology/immunohistochemistry, approximately 50 laser spots were applied. All rats were killed by transcardial perfusion with physiological saline under deep anesthesia; and the globes were enucleated immediately for analysis by histology, immunohistochemistry, Western immunoblotting, RT-PCR, or terminal deoxynucleotidyl transferase-mediated–dUTP nick-end labeling (TUNEL) assay (see below).

Table 1. Definitions of Lasers and Their Energy Settings

Laser	Pulse Duration	Energy Setting	Radiant Exposure, J/cm^2/pulse
2RT-L	3 ns	0.21 mJ	0.106
2RT-H	3 ns	0.33 mJ	0.166
CW	100 ms	90 mW	12.7

Two cohorts of rats were used in the current study. The first cohort was used for immunohistochemistry/histology. The number of eyes analyzed at each time point was as follows: 6 hours ($n = 6$), 1 day ($n = 10$), 3 days ($n = 10$), 7 days ($n = 10$). The second cohort was used for RT-PCR and Western immunoblotting. The number of eyes analyzed per treatment group at each time point was as follows: 6 hours ($n = 9$), 1 day ($n = 9$), 3 days ($n = 9$), 7 days ($n = 9$). A further group of untreated rats ($n = 9$) served as controls.

Tissue Processing and Histology

Eyes that were subsequently used for toluidine blue staining were immersion fixed in 2.5% glutaraldehyde with 4% paraformaldehyde in 0.1 M phosphate buffer, pH 7.4, for 24 hours at 4°C. They were then placed in 2% osmium tetroxide in saline overnight and washed with sodium cacodylate buffer (140 mM, pH 7.2) at room temperature. Subsequently, the tissue was dehydrated in graded alcohols and embedded in epoxy resin (TAAB Embedding Resin; TAAB Laboratories, Aldermaston, Berkshire, UK) for transverse sectioning. Sections (0.75 μm) were cut on an ultramicrotome, mounted on glass slides, and osmium tetroxide–induced myelin staining enhanced using 1% toluidine blue.

Eyes that were subsequently used for hematoxylin and eosin (H&E)/immunohistochemistry/TUNEL labeling were immersion fixed in Davidson's solution for 24 hours, then transferred to 70% ethanol until processing. Davidson's solution, which comprises two parts formaldehyde (37%), three parts 100% ethanol, one part glacial acetic acid, and three parts water, is the preferred fixative for whole eyes as it provides optimal tissue morphology while avoiding retinal detachment. Whole eyes were then hand processed as described previously.[37] Globes were embedded in a sagittal orientation, and 4 μm sections were cut.

Eyes that were subsequently used for whole-mount immunohistochemistry were dissected into posterior eye cups and then postfixed by immersion in 4% paraformaldehyde (PFA) for 1 hour. For retinal whole mounts, retinas were gently dissected free and prepared as flattened whole mounts by making four radial cuts. For RPE–choroid–sclera whole mounts, the retina was carefully removed from the posterior eye cup, which was then subjected to eight radial cuts to ensure a flat RPE preparation.

Immunohistochemistry

Immunohistochemistry of transverse retinal sections was performed as previously described.[37,38] In brief, tissue sections were deparaffinized and treated with H_2O_2 to block endogenous peroxidase activity.

Table 2. Antibodies Used in the Study

Target	Host	Clone/Catalog No.*	Dilution	Source
Brn3a	Goat	sc-31,984	1:3000, 1:1000†	Santa Cruz Biotechnology Inc., Dallas, TX
Calbindin	Mouse	CB-955*	1:1000, 1:1000†	Sigma-Aldrich, Castle Hill, New South Wales, Australia
Calretinin	Rabbit	AB5054	1:2500, 1:1000†	Merck Pty Ltd., Kilsyth, Victoria, Australia
Laminin	Rabbit	AT 2404	1:3000	E Y Labs, San Mateo, CA
MCT-3	Rabbit	MCT-35 A	1:750, 1:500‡	Alpha Diagnostic International, San Antonio, TX
Nestin	Mouse	Rat 401*	1:200‡	Becton Dickenson, North Ryde, New South Wales, Australia
PKCα	Mouse	MC5*	1:1000, 1:1000†	Abcam, Cambridge, UK
Rhodopsin	Mouse	RET-P1*	1:600	Abcam
RPE-65	Mouse	8B11*	1:3000, 1:500‡	Santa Cruz Biotechnology Inc.
ZO-1	Rabbit	61-7300	1:200‡	Invitrogen, Mulgrave, Victoria, Australia

* Clone number.
† Western immunoblotting.
‡ Immunofluorescence.

Antigen retrieval was then achieved by microwaving the sections in 1 mM EDTA buffer (pH 8.0). Subsequently, tissue sections were blocked in PBS and were incubated overnight at room temperature in primary antibody (see Table 2), followed by consecutive incubations with biotinylated secondary antibody and streptavidin–peroxidase conjugate. Color development was achieved using NovaRED substrate kit (Vector Laboratories Inc., Burlingame, CA) for 3 minutes. Sections were counterstained with hematoxylin and subsequently mounted. In order to evaluate specificity of antibody labeling, adjacent sections were incubated with the appropriate isotype control for monoclonal antibodies or normal rabbit/goat serum for polyclonal rabbit/goat antibodies. In addition, Western blotting was performed for the majority of the antibodies in order to confirm that they recognized targets with the appropriate molecular masses. Confirmation of the specificity of antibody labeling was judged by the morphology and distribution of the labeled cells, by the absence of signal when the primary antibody was replaced by isotype/serum controls, by comparison with the expected staining pattern based on our own and other previously published results, and by the presence within retinal samples of a Western blot band of the expected molecular weight.

For immunofluorescence of RPE whole mounts, samples were rinsed with PBS, permeabilized with PBS containing 0.5% Triton (PBS-T), blocked in PBS-T containing 3% normal goat serum, and then incubated in the same solution additionally containing anti-ZO-1 or anti-RPE-65 primary antibody (see Table 2 for details) overnight at 4°C. After further washing with PBS, the appropriate AlexaFluor 488–conjugated secondary antibody (Invitrogen) was applied to each whole mount for 3 hours at room temperature. Whole mounts were then rinsed in PBS, mounted using antifade mounting medium, and examined under a confocal fluorescence microscope (BX-61; Olympus, Mount Waverly, Victoria, Australia). For double-labeling immunofluorescence of retinal whole mounts, samples were treated exactly as described above except that a combination of anti-Brn3a plus antinestin primary antibodies or anticalretinin plus antinestin primary antibodies was used (see Table 2 for details). On the following day, whole mounts were incubated with the appropriate combination of AlexaFluor 488– and AlexaFluor 594–conjugated secondary antibodies.

Quantification of Cell-Specific Immunohistochemical Labeling

Due to the irregular appearance and therefore inconsistent number and/or orientation of laser lesions in transverse retinal preparations, it was not considered meaningful to quantify all of a given type of labeled cell in one complete section. Instead, by carefully cutting serially through eyes, each individual laser-induced lesion could be identified and sections found that passed approximately through the center of such regions. By initially employing an eyepiece graticule and stage micrometer (Graticules Ltd., Tonbridge, Kent, UK) to define distance, we delineated a region that extended 500 μm on each side of the central point of a laser lesion (this essentially equated to one microscopic field, using the ×20 objective, and included both lesion site and surrounding region to ensure that all local effects were observed). Within this region we quantified the number of specifically immunolabeled cells (e.g., for Brn3a, PKCα, calbindin, calretinin) and defined these as being typical of a particular type of cell in the region (e.g., Brn3a for ganglion cells, PKCα for ON bipolar cells). Areas of retina on the same section that did not fall within 2 mm of a laser lesion were assessed for "control" cell counts.

TUNEL Assay

TUNEL assays were performed as previously described.[39] In brief, sections were deparaffinized, rehydrated, and treated with proteinase K. Endogenous peroxidases were inactivated by incubation in H_2O_2. Sections were equilibrated in TdT buffer (30 mM Tris-HCl, pH 7.2, containing 140 mM sodium cacodylate, 1 mM cobalt chloride) prior to incubation in the same buffer containing TdT (0.15 U/μL) and biotin-16-dUTP (10 μM). The reaction was terminated by two washes in saline sodium citrate solution. Nonspecific binding sites were blocked using bovine serum albumin prior to incubation of sections with streptavidin–peroxidase conjugate. Color development was achieved using a NovaRED substrate kit (Vector Laboratories Inc.). Sections were counterstained with hematoxylin and subsequently mounted.

Western Immunoblotting of Retinal Extracts

Western blotting was undertaken as described previously.[40] In brief, tissue extracts were sonicated in homogenization buffer (20 mM Tris-HCl, pH 7.4, 25°C, containing 2 mM EDTA, 0.5 mM EGTA, 1 mM dithiothreitol, 50 μg/mL leupeptin, 50 μg/mL pepstatin A, 50 μg/mL aprotinin, and 0.1 mM phenylmethylsulphonyl fluoride). An equal volume of sample buffer (62.5 mM Tris-HCl, pH 7.4, containing 4% SDS, 10% glycerol, 10% β-mercaptoethanol, and 0.002% bromophenol blue) was then added, and samples were boiled; protein concentrations in each sample were equalized with the bicinchoninic acid (BCA) assay.[41] Electrophoresis was performed on denaturing polyacrylamide gels (7.5%, 10%, or 12%, as appropriate), after which proteins were transferred to polyvinylidine fluoride membranes for immunoprobing. Membranes were incubated with the appropriate antisera (as detailed in Table 1) overnight, and labeling was carried out using a two-step detection procedure: First, appropriate biotinylated secondary antibodies (1:500; 30 minutes) were reacted with membranes, and then streptavidin–peroxidase conjugates were applied. Positive antibody labeling was detected as described previously,[40] and quantification of

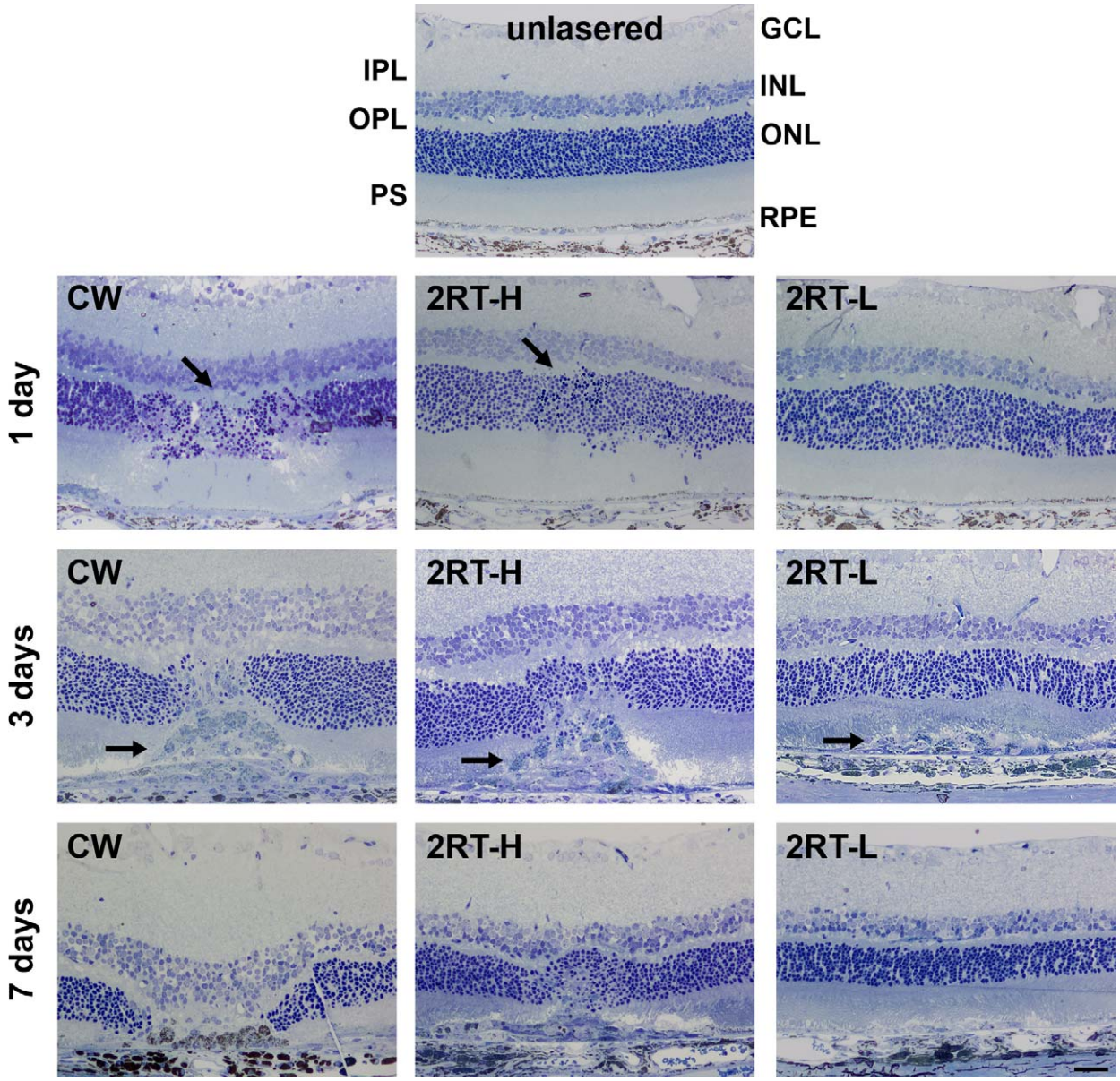

Figure 1. Representative images of retinal histology following treatment with CW or 2RT laser, used at high (2RT-H) and low (2RT-L) energy settings, as delineated by toluidine blue staining of transverse sections. At 1 day after laser treatment, damage to the ONL (*arrows*) is evident within the CW retina and, to a much lesser extent, the 2RT-H retina. By 3 days after laser treatment, substantial destruction of the ONL is apparent within the lesion site of the CW retina, while very limited loss of ONL neurons is detectable in the 2RT-H retina. Proliferating/infiltrating cells are visible within CW, 2RT-H, and 2RT-L retinas (*arrows*). By 7 days after laser treatment, retinal damage has partially resolved. *Scale bar*: 30 μm. GCL, ganglion cell layer; IPL, inner plexiform layer; INL, inner nuclear layer; OPL, outer plexiform layer; ONL, outer nuclear layer; PS, photoreceptor segments.

detected proteins was achieved using Adobe Photoshop CS2 (Adobe Australia, Sydney, New South Wales, Australia). Detection of β-actin was assessed in all samples as a positive gel-loading control.

Results

Effects on Retinal Morphology

The effect of the CW laser on retinal morphology was profound (Fig. 1). In comparison with nontreated regions of the rat retina, a definite pattern of damage could be discerned. One day after CW laser irradiation, the outer retina (particularly the photoreceptor outer segments, the RPE layer, and the outer nuclear layer [ONL]) appeared disorganized and vacuolar; the normal, neat cellular stratification was no longer obvious, and the ONL appeared swollen and disparate. After 3 days, substantial destruction of the ONL and outer segments was evident; this was accompanied by the presence of additional cells in what was previously the interphotoreceptor matrix region, which were likely either proliferating or infiltrating cells (Fig. 1). By 7 days after irradiation, there was a complete loss of photoreceptors and infiltration into this tissue region by pigmented cells perhaps derived from the RPE cell layer. The overlying inner nuclear layer (INL) was swollen, and cells also appeared to be migrating from this region to fill the void left by the destruction of the photoreceptors.

At the high setting (2RT-H), the 2RT laser produced a minor but discernible effect when retinas were viewed 24 hours after

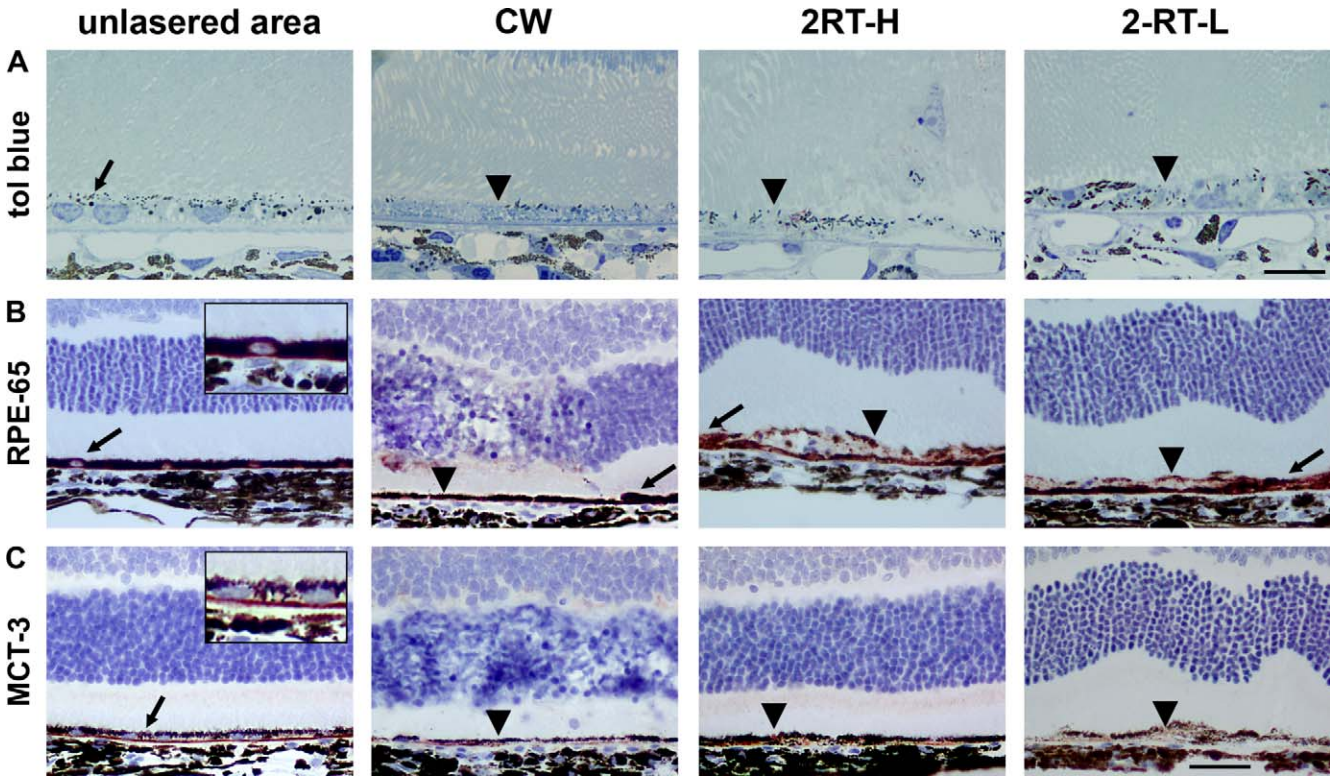

Figure 2. Representative images of the RPE at 1 day following treatment with CW or 2RT laser, used at high (2RT-H) and low (2RT-L) energy settings, as delineated by toluidine blue staining (**A**) and immunohistochemistry for RPE-65 (**B**) and MCT-3 (**C**) in transverse sections. (**A**) Histology demonstrates a dearth of RPE cells at the lesion in all three laser treatment groups (*arrows*) when compared with an unlasered area (*arrowhead*). (**B**, **C**) In the normal eye, RPE-65 labels the cytoplasm of RPE cells, while MCT-3 selectively demarcates the basolateral membrane (*arrows*, *insets*). In all three laser treatment groups, disruption to and thinning of RPE-65 and MCT-3 can be seen (*arrrowheads*) at the lesion when compared to adjacent regions (*arrows*). *Scale bar*: 12 μm (**A**); 30 μm (**B**, **C**).

laser irradiation. There was a slight disturbance to the ONL, including the presence of some obvious pyknotic nuclei. Some displaced cells were also present within the photoreceptor outer segment layer (Fig. 1). By 3 days after laser treatment, there was a readily discernible disruption to the structure of the ONL. This included some cell nuclear loss and a minor thinning of the outer segment layer. Infiltrating cells were noted in the subretinal space, but there were not as many as after CW laser treatment. By 7 days after treatment there was no further damage; invading cells were still present in the subretinal space, but no further disruption to the ONL was noted. In contrast to the 2RT-H setting, the lower setting of the 2RT laser (2RT-L) had little obvious effect on retinal morphology after 1 day (Fig. 1). After 3 and 7 days some infiltrating cells could be seen in the subretinal space, but there was no discernible disruption to the ONL.

Effects on RPE Cells and Bruch's Membrane

Detailed histologic analysis of outer retinas 24 hours subsequent to irradiation with either CW or the 2RT laser (high and low settings) revealed that in each case there was a significant destruction of the RPE cellular monolayer due to the loss of individual cells, as compared with nontreated areas (Fig. 2A). RPE antigen-specific immunohistochemistry confirmed these findings: 24 hours after each laser treatment, immunoreactivities for both RPE-65, which labels the cytoplasm (Fig. 2B), and MCT-3, which labels the basolateral membrane (Fig. 2C), were diminished in intensity as compared with nontreated regions. Furthermore, the thickness of each positive layer of immunoreactive label was also reduced, and generally, immunolabeling had become much more disorganized (Figs. 2B, 2C).

Whole-mount preparations in which RPE cells were labeled for cytoplasmic RPE-65 (Fig. 3A) and the tight junction marker ZO-1 (Fig. 3B) showed close agreement with the data shown in Figure 2: Postlaser lesion sites were seen in the RPE monolayer that corresponded with the diameter of the irradiating laser beam. The data in Figures 2 and 3 together indicate that treatment with the CW laser or the 2RT laser (at high or low settings) produced such lesions.

In order to investigate the integrity of Bruch's membrane after laser irradiation, transverse retina/RPE sections were labeled with the basement membrane component laminin. Normal laminin immunoreactivity is clearly associated with Bruch's membrane (Fig. 4A). After treatment with either the CW laser (Fig. 4B) or the 2RT laser at the higher setting (2RT-H; Fig. 4C), there was obvious disruption to the RPE and associated photoreceptor outer segments, as previously shown. Importantly, however, in each case Bruch's membrane remained intact.

Interestingly, by 7 days after laser treatment, RPE cells, as shown by immunolabeling with RPE-65, had migrated back into lesion sites (Fig. 5). This was the case with all three lasers and provided further proof that the basement membrane remained physiologically intact.

Death of Photoreceptors and Association with TUNEL Labeling

In non–laser-treated areas of retina there were essentially no TUNEL-positive cells present (not shown). At 24 hours after

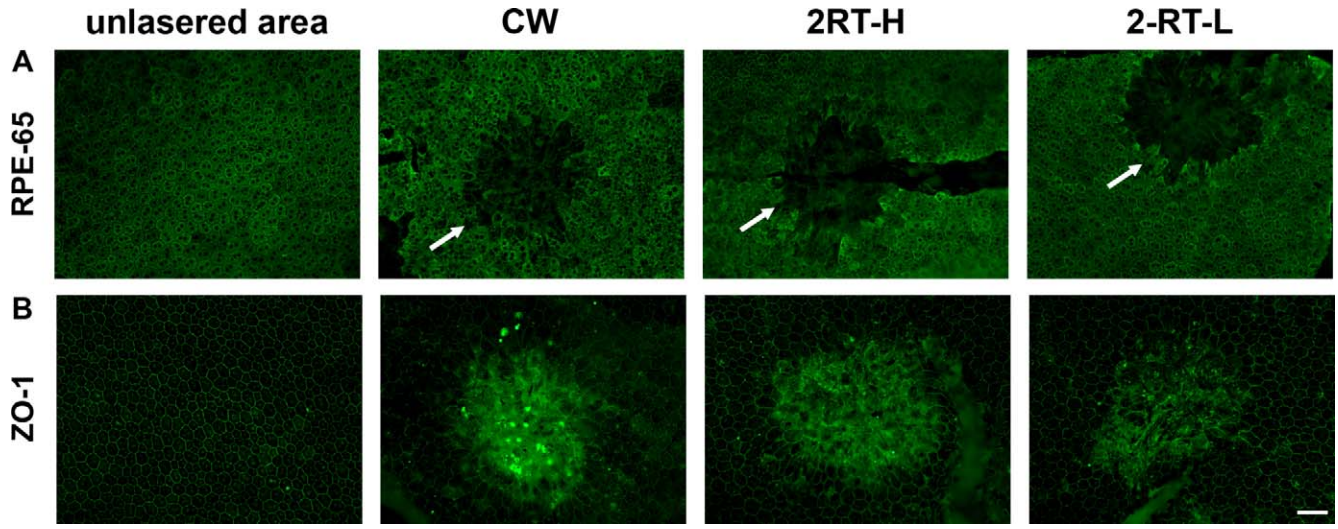

Figure 3. Representative images of the RPE cell layer at 3 days following treatment with CW or 2RT laser, used at high (2RT-H) and low (2RT-L) energy settings, as shown by immunohistochemistry for RPE-65 (**A**) and ZO-1 (**B**) in RPE whole mounts. In unlasered areas, RPE-65 expression is cytoplasmic, while ZO-1 expression is restricted to tight junctions. Both *markers* highlight the "honeycomb" structure of the RPE layer. In all three laser treatment groups, lesion sites are clearly visible with loss of and disruption to the patterns of RPE-65 and ZO-1 immunoreactivities (*arrows*). *Scale bar*: 30 μm.

irradiation with the CW laser, however, approximately 95% of nuclei in the ONL in the treated zone were labeled as TUNEL positive (Fig. 6A). Many ONL nuclei were also labeled at this time in the 2RT-H retinas, although significantly fewer than with the CW laser (approximately 50% of those in the irradiated region). In 2RT-L retinas, some TUNEL-positive nuclei were discerned within this cell layer, but in a negligible amount compared with either the CW laser or the 2RT-H setting (Fig. 6A). The actual numbers of TUNEL-positive nuclei in the irradiated zone were quantified as shown in Figure 6C; the value obtained for the CW laser was significantly greater ($P < 0.01$) than for both the 2RT-H and the 2RT-L laser.

Since the presence of TUNEL labeling in the ONL 24 hours subsequent to irradiation implied that photoreceptors were being lost, changes in these cells were assessed after 3 days to see if this was indeed the case (Fig. 6B). Immunolabeling of retinas after each laser treatment showed a loss of rhodopsin immunoreactivity that corresponded with the increased TUNEL labeling (Fig. 6B). In the case of the CW laser there was an almost complete loss of rhodopsin labeling in the irradiated zone, which indicated that all of the TUNEL-positive cells noted in the ONL after 24 hours had indeed been lost. For the 2RT-H setting, there was a loss of approximately 50% of the rhodopsin labeling, again corresponding to the observed amount of TUNEL detected. In the case of the 2RT-L setting, where only sporadic individual TUNEL-positive nuclei were detected (Fig. 6A), only a small loss of rhodopsin could be detected, and this was solely from the outer segments (Fig. 6B).

Effects on Retinal Neurons

Four distinct classes of retinal neurons were assessed: horizontal cells, rod bipolar cells, amacrine cells, and ganglion cells (RGCs). These were identified by immunohistochemical analysis of retinas with four separate antibodies that have specific labeling patterns (calbindin, PKCα, calretinin, and Brn3a, respectively). All retinas were analyzed 7 days after laser irradiation so that any putative loss of neurons via both rapid and delayed cell death would be detected.

Calbindin-Positive Horizontal Cells. Figure 7 shows the effects of each type of laser treatment on retinal horizontal cells as labeled by calbindin immunoreactivity. In nontreated retinas, calbindin is ordinarily associated with horizontal cell somata at the outer edge of the INL and with a single stratum of dendrites in the outer plexiform layer (Fig. 7A). Although the morphological appearance of the retina was altered to differing degrees by the CW laser (Fig. 7B) and the 2RT laser (2RT-H, Fig. 7C; 2RT-L, Fig. 7D) as described above, and this necessarily affected the shape of the horizontal cells and their dendrites, there was essentially no change in the amount or

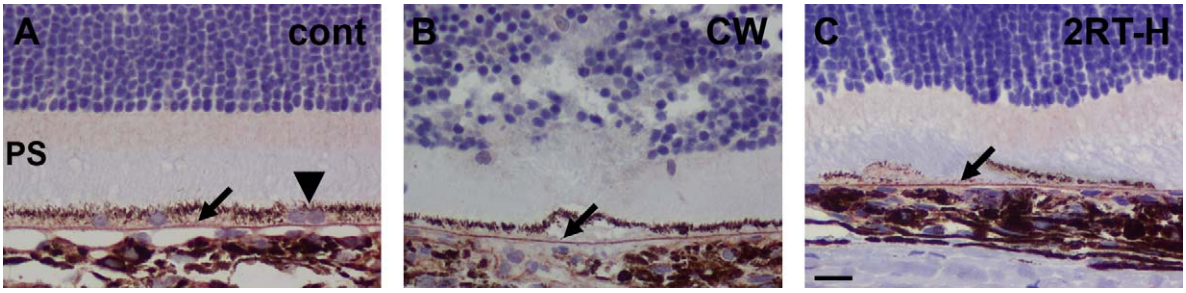

Figure 4. Analysis of Bruch's membrane following treatment with CW or 2RT laser, used at the high (2RT-H) energy setting, as determined by immunohistochemistry for laminin. In the normal retina (**A**), laminin demarcates Bruch's membrane (*arrow*), situated basal to the RPE cell layer (*arrowhead*). At 1 day after laser treatment, Bruch's membrane appears intact (*arrows*) in the CW (**B**) and 2RT-H (**C**) retinas in spite of damage suffered by the RPE cell layer. *Scale bars*: 15 μm. PS, photoreceptor segments; cont, untreated control.

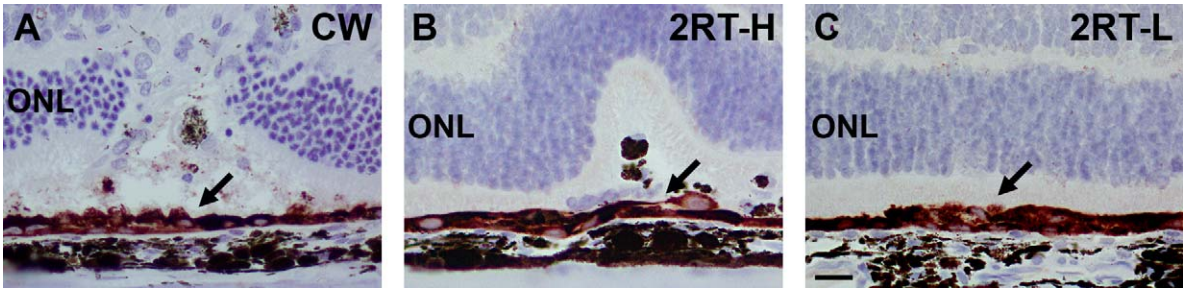

Figure 5. Analysis of RPE status 7 days after focal irradiation of retinas with either CW laser (**A**), 2RT laser at the high setting (2RT-H) (**B**), or 2RT laser at the lower energy setting (2RT-L) (**C**), as denoted by immunolabeling of this cellular monolayer with the anti-RPE-65 antibody. It is clearly visible that RPE cells are once again present in lesioned areas (*arrows*) in each case. *Scale bars*: 15 μm. ONL, outer nuclear layer.

subcellular distribution of calbindin after any of the treatments. This was confirmed by data quantifying perikaryal numbers (see Fig. 11) and overall retinal levels of calbindin by immunoblot analysis (see Supplementary Material and Supplementary Fig. S1, http://www.iovs.org/lookup/suppl/doi:10.1167/iovs.12-11203/-/DCSupplemental).

PKCα-Positive Rod Bipolar Cells. Analysis of rod bipolar cells was undertaken by immunolabeling with PKCα. In untreated retinas, this label is associated with bipolar cell perikarya located at the outer extremes of the INL, their axonal processes that longitudinally traverse the INL and inner plexiform layer (IPL), and their terminals in and around the ganglion cell layer (GCL; Fig. 8). None of the tested laser treatments altered the quantity or subcellular localization of PKCα in either cell bodies or terminals (Fig. 8), or the overall quantity of this protein (see Fig. 11; see Supplementary Material and Supplementary Fig. S1, http://www.iovs.org/lookup/suppl/doi:10.1167/iovs.12-11203/-/DCSupplemental). Treatment with the CW laser, however, caused a clear loss of the axonal PKCα labeling and an enhancement of labeling in the terminals, but this phenomenon was evident solely in the irradiated zone (Fig. 8).

Calretinin-Positive Amacrine Cells. In untreated retinas, characteristic calretinin immunoreactivity was present in amacrine cell perikarya in the innermost level of the INL, in three strata of terminals and dendrites within the IPL, and in neurons of the GCL (Fig. 9A). From analysis of retinas 7 days after laser irradiation, it was clear that calretinin immunoreactivity was largely unaffected by all of the treatment regimens (Fig. 9). There was no obvious loss of perikarya or dendritic/terminal labeling in all cases. Analysis of retinal whole mounts that had also been labeled with calretinin showed no alteration in labeling distribution or quantity in either CW-induced or 2RT-H-induced lesion sites as compared with nonirradiated regions (Fig. 9B). Note that laser-induced lesions were visualized by labeling for the inducible intermediate filament protein nestin. When calretinin immunoreactivity was quantified by counting numbers of perikarya in the INL from representative transverse retinal sections (see Fig. 11), there was no alteration in numbers after any of the laser treatments. This was also the case when calretinin levels were quantified in retinas after each treatment by Western immunoblot analysis (see Supplementary Material and Supplementary Fig. S1, http://www.iovs.org/lookup/suppl/doi:10.1167/iovs.12-11203/-/DCSupplemental).

Brn3a-Positive Retinal Ganglion Cells. In transverse sections of untreated retinas, Brn3a can clearly be identified in a subset of RGC nuclei (Fig. 10A). It was evident that at 7 days following any of the laser treatments, there were no obvious alterations in either distribution or magnitude of Brn3a labeling in regions of the retina overlying or neighboring lesions (Fig. 10). Moreover, there was also no change in the numbers of Brn3a-immunoreactive RGCs in lesioned areas compared with untreated tissue regions (Fig. 11). Western immunoblot analysis of treated retinas showed agreement with these data: There was no significant alteration in the level of Brn3a in any of the laser-treated retinas as compared with controls (see Supplementary Material and Supplementary Fig. S1, http://www.iovs.org/lookup/suppl/doi:10.1167/iovs.12-11203/-/DCSupplemental).

Discussion

The present study was designed to fulfill two major aims. The first was to characterize the detailed histologic and cellular damage profiles resulting from a clinically relevant retinal photocoagulation treatment with a standard CW laser to pigmented rat eyes. The second was to compare these data with those obtained from parallel studies using the much shorter-duration nanosecond pulse 2RT laser. Our previously conducted in vitro studies demonstrated that the 2RT laser could ablate the RPE without significant collateral damage to the retina.[19] In the current study we sought to ascertain whether this was also the case in vivo.

Traditional, CW-Applied Laser Photocoagulation

Treatment of retinas with the conventional CW laser at a clinically relevant energy level caused the rapid appearance of significant lesions that were associated with ablated RPE, induction of both instant and delayed photoreceptor death, and widespread edema. It was also evident that even though RPE cells in the irradiated regions were killed, there was no associated destruction of the underlying Bruch's membrane. This is significant because it theoretically allows for the replacement of dead RPE by either migration or proliferation of cells from outside of the lesion site. In fact, this was borne out by the present data: By 7 days after laser treatment, new RPE cells were typically found overlying Bruch's membrane within lesion sites. This is in agreement with work by von Leithner and colleagues, who have shown that induction of focal laser-induced lesions in the RPE layer cause a global proliferative drive in these cells, which lasts for several days, in order to repair the damage.[42] Roider and colleagues have reported similar observations in rabbits after laser photocoagulation, namely that reestablishment of the RPE monolayer was essentially in place by 3 days after laser treatment and that this event was coincident with a reduction in local edema.[28] As stated previously, it is not clear where the beneficial influence for retinal laser photocoagulation actually lies, but certainly the stimulation of RPE cells located away from the lesion site in the present study represents a significant tissue response. The RPE are likely being driven to alter their physiological functions by

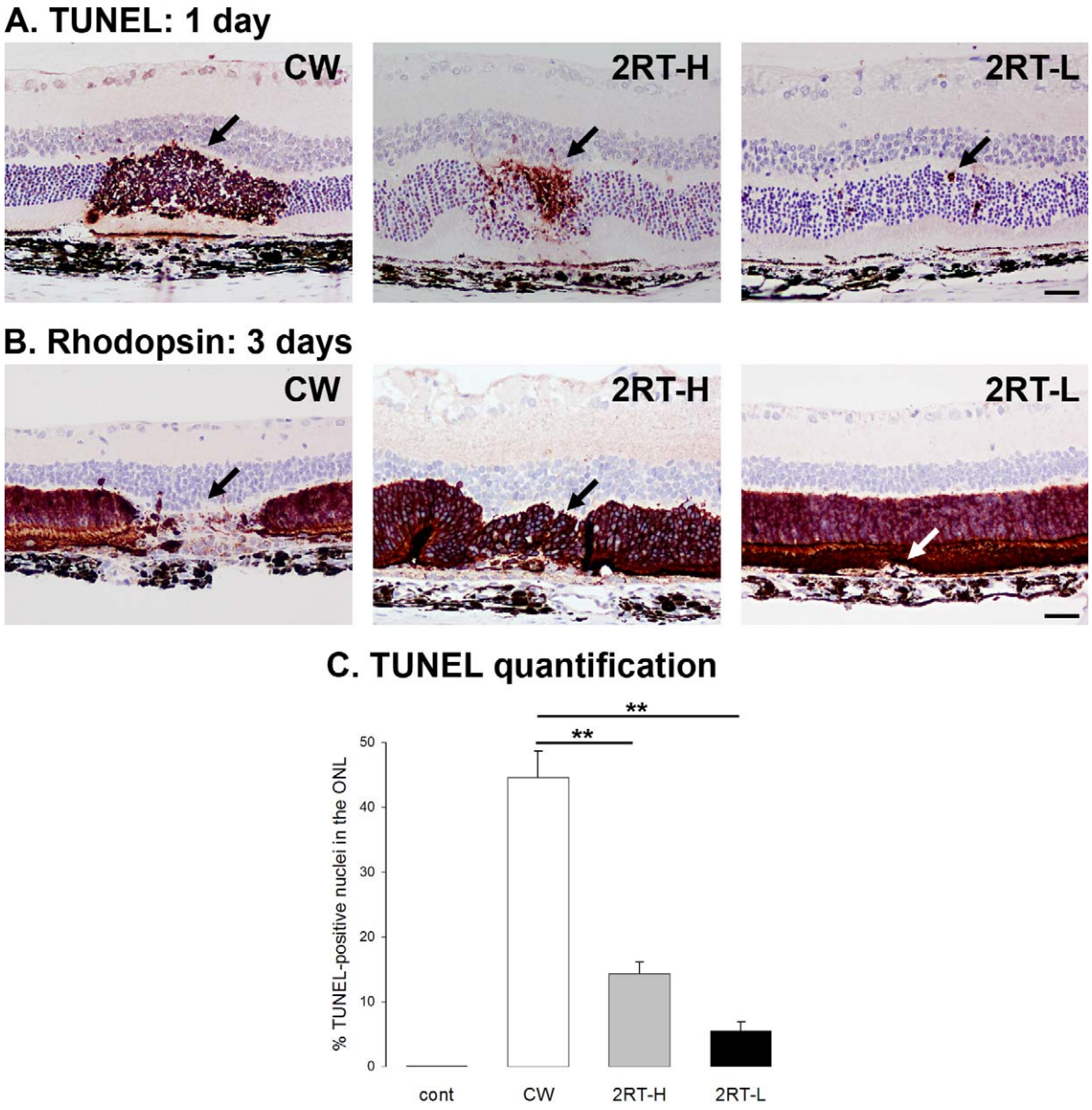

Figure 6. TUNEL labeling and photoreceptor cell death following treatment with CW or 2RT laser, used at high (2RT-H) and low (2RT-L) energy settings. (**A**) Representative images of TUNEL labeling at 1 day after laser treatment. (**B**) Representative images of photoreceptors at 3 days after laser treatment, as shown by immunohistochemistry for rhodopsin. The CW retina features intense TUNEL reactivity in the ONL and a corresponding loss of virtually all rhodopsin-labeled cells at the lesion (*arrows*). In the 2RT-H retina, a proportion of cells in the ONL are TUNEL positive with an equivalent reduction in rhodopsin (*arrows*), while in the 2RT-L retina, TUNEL-positive cells are rare (*black arrow*) and the only alteration to rhodopsin immunolabeling is at the level of the outer segments (*white arrow*). *Scale bar*: 30 μm. GCL, ganglion cell layer; INL, inner nuclear layer; ONL, outer nuclear layer. (**C**) Quantification of TUNEL labeling at 1 day after laser treatment. Data are expressed as the mean ± SEM, where $n = 10$ to 14. $^{**}P < 0.01$, by ANOVA followed by post hoc Tukey's test.

factors released as a result of laser injury. Such factors, for example platelet-derived growth factor (PDGF),[43] VEGF,[44] or pigment epithelium-derived factor (PEDF),[45,46] can be released by surviving RPE cells that have been either directly or indirectly physically or chemically stressed. These factors could also, obviously, have effects on other local non-RPE cell types too, and these latter influences would also likely contribute to the overall retinal response to laser photocoagulation. Other mechanisms for the therapeutic potential of laser photocoagulation have been mooted; these include the alteration of immune cell signaling and activity, vascular thrombosis, and improvements in transport across Bruch's membrane.[27,47–53] Indeed, it has been suggested that the establishment of a new RPE layer at the laser lesion site, with a dilution of the intracellular debris that is known to accumulate with aging,[54] will restore the efficiency of the blood–retinal barrier, and that this is what provides the therapeutic benefit of laser photocoagulation.[55] The RPE layer repair seen in the present study would add some support to this theory. Finally, an interesting study from Machalinska and colleagues has also shown that bone marrow–derived stem cells are mobilized to the retina in response to RPE damage and that these could provide factors that contribute to the local repair processes.[56]

The most obvious histologic change seen as a result of laser photocoagulation with the CW laser was within the outer retina, where localized destruction of photoreceptors, appearance of

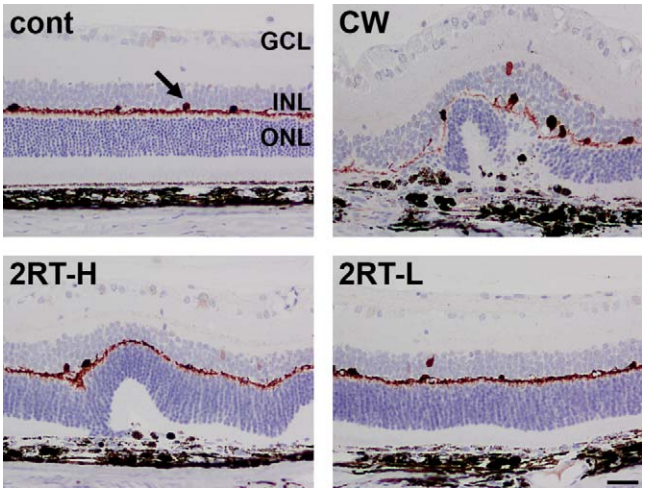

Figure 7. Representative images of horizontal cells following treatment with CW or 2RT laser, used at high (2RT-H) and low (2RT-L) energy settings, as shown by immunohistochemistry for calbindin (*arrow*). In the normal retina (cont), calbindin is associated with horizontal cell somata located in the outer part of the INL and their dendrites in the outer plexiform layer. At 7 days after laser treatment, calbindin immunoreactivity is largely unaffected in the CW, 2RT-H, or 2RT-L retinas when compared to controls. *Scale bar*: 30 μm. GCL, ganglion cell layer; INL, inner nuclear layer; ONL, outer nuclear layer.

extensive edema, and loss of the overall tissue architecture were apparent. The destructive effect of the CW laser on photoreceptors is well known, and our findings are in good agreement with previous histologic studies.[15,23,25–27,57–59] This effect underlies the disadvantage of using retinal photocoagulation for treatment of DME: Photoreceptor damage has been reported to be irreversible and progressive, resulting in visual scotomae,[2,18,60] yet photoreceptor death appears not to be necessary for resolution of edema.[16,18,20,61] In the present study, the

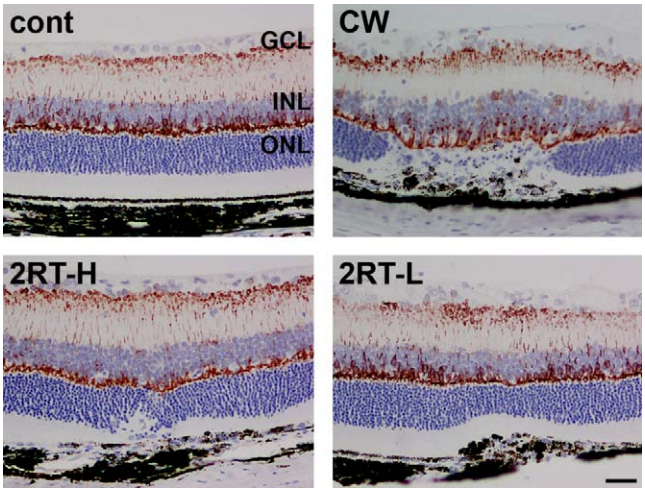

Figure 8. Representative images of bipolar cells following treatment with CW or 2RT laser, used at high (2RT-H) and low (2RT-L) energy settings, as shown by immunohistochemistry for PKCα. In the normal retina (cont), PKCα is associated with bipolar cell somata located in the outer part of the INL and their processes that synapse with photoreceptors and RGCs. At 7 days after laser treatment, PKCα immunoreactivity is largely unaffected in the CW, 2RT-H, or 2RT-L retinas when compared to controls. *Scale bar*: 30 μm. GCL, ganglion cell layer; INL, inner nuclear layer; ONL, outer nuclear layer.

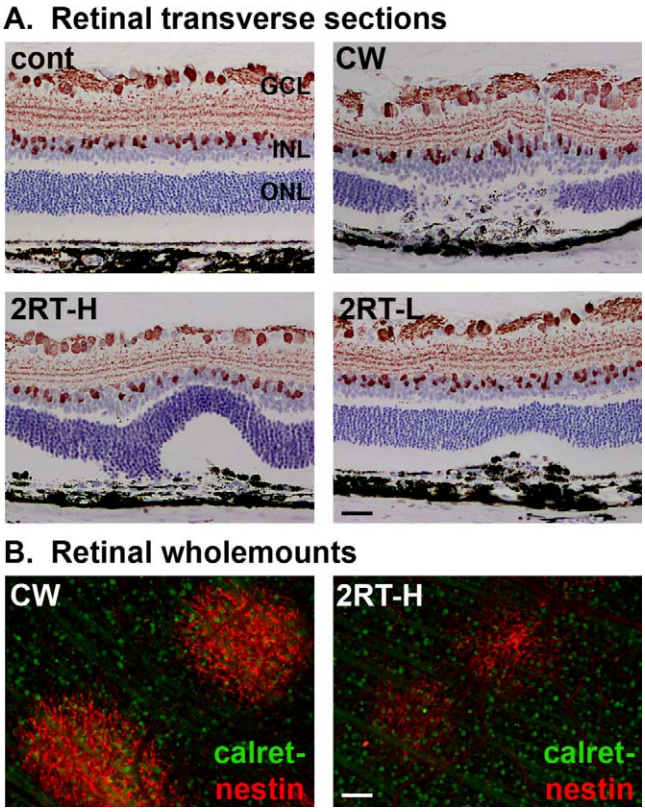

Figure 9. Representative images of amacrine cells following treatment with CW or 2RT laser, used at high (2RT-H) and low (2RT-L) energy settings, as shown by immunohistochemistry for calretinin. (**A**) Calretinin immunolabeling in transverse sections. In the normal retina, calretinin is associated with amacrine cell somata located in the inner part of the INL, three layers of terminals visible in the IPL, and various neurons in the GCL. At 7 days after laser treatment, calretinin immunoreactivity is largely unaffected in the CW, 2RT-H, or 2RT-L retinas when compared to controls. (**B**) Double-labeling immunofluorescence of calretinin with nestin in CW- and 2RT-H-treated whole mounts analyzed after 3 days. The pattern of calretinin-positive neurons and axons (*green*) is unaffected in lesioned areas, indicated by upregulated nestin expression (*red*). *Scale bars*: 30 μm. GCL, ganglion cell layer; INL, inner nuclear layer; ONL, outer nuclear layer; calret, calretinin.

detection of TUNEL-positive (i.e., apoptosing) cell nuclei was confined to the photoreceptor layer of the neuroretina. Furthermore, the decreases in the levels of rhodopsin protein had reached a plateau by 3 days after treatment, meaning that photoreceptor degeneration had ceased by this point. Data from other researchers have shown that denuded regions of the ONL are slowly repaired after laser photocoagulation by endogenous mechanisms.[23,27,58,62] This process is thought to occur principally via migration of neighboring photoreceptors, but migration and dedifferentiation of Müller cells may also play a part. It is uncertain whether restoration of ONL continuity results in any reinstatement of local function or whether microscotomas persist indefinitely.

Little convincing evidence was found in the present study to show that the neuron classes analyzed in the inner retina were detrimentally affected by CW laser photocoagulation. Analyses indicated that calbindin-positive horizontal cells, calretinin-positive amacrine cells, and Brn3a-positive RGCs were not damaged, even when overlying the lesion. The first two markers are calcium-binding proteins, decreased or altered expression of which could indicate aberrant calcium buffering; Brn3a is a transcription factor controlling development,

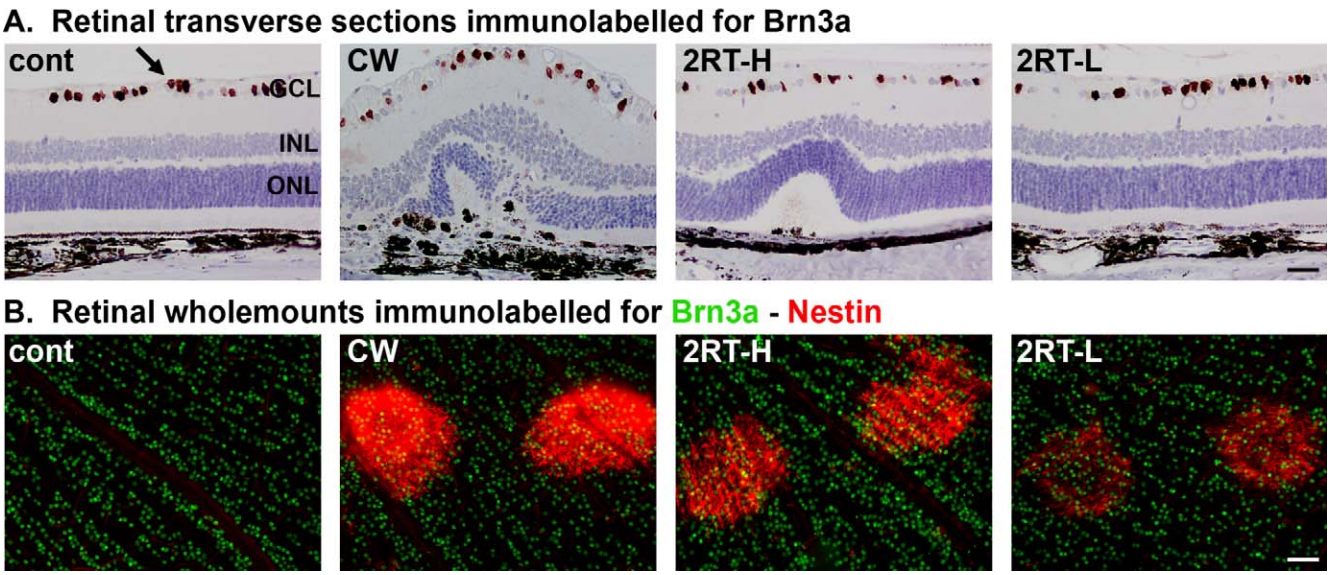

Figure 10. Representative images of RGCs following treatment with CW or 2RT laser, used at high (2RT-H) and low (2RT-L) energy settings, as shown by immunohistochemistry for Brn3a. (**A**) Brn3a immunolabeling in transverse sections. In the normal retina, Brn3a is exclusively associated with RGC nuclei located in the GCL (*arrow*). At 7 days after laser treatment, Brn3a immunoreactivity is largely unaffected in the CW, 2RT-H, or 2RT-L retinas when compared to controls. (**B**) Double-labeling immunofluorescence of Brn3a with nestin in control and lasered whole mounts analyzed after 3 days. The pattern of Brn3a-positive neurons (*green*) is unaffected in lesioned areas, indicated by upregulated nestin expression (*red*). *Scale bars*: 30 μm. GCL, ganglion cell layer; INL, inner nuclear layer; ONL, outer nuclear layer.

morphology, and function of RGCs[63] that has been shown to be downregulated soon after injury. The unaltered patterns of expression provide evidence that these neurons are morphologically and functionally healthy following laser treatment. The only apparent effect was that the induction of swelling and edema in the outer retina at lesion sites caused some physical displacement of overlying neurons. This was particularly apparent in the case of the calbindin-positive horizontal cells, which reside physically closer to the outer retina and are therefore more obviously pulled at by locally generated tractional forces resulting from the swelling and inflammation of adjacent tissue. This effect was also described by Marshall, who stated that thermal damage was confined to the RPE and photoreceptors, with disturbances to inner retinal layers resulting secondarily from indirect mechanical disturbances.[25] Interestingly, a previous detailed analysis of the response of the rabbit retina to laser photocoagulation showed microglial-associated delayed axonal degeneration in the nerve fiber layer in the week following treatment.[33] This demonstrates that RGCs can be detrimentally affected by laser photocoagulation in some instances, although this was not the case in the present study. However, the rabbit retina does not resemble that of the rat, lacking a general retinal blood supply.[64] Furthermore, the present laser was used at a power setting not dissimilar to those used in the clinic, and produced burns of commensurate grade. This power setting is substantially lower than the energy levels used in the previous study (180–200, 350–400 mW).[33] We therefore believe we have shown that use of the CW laser is unlikely to detrimentally affect inner retinal neurons in the clinical setting if energy settings are employed that result in ophthalmic burns no greater in intensity than those observed in this study.

PKCα, an enzyme specifically localized to cell bodies, axons, and terminals of mammalian rod bipolar cells, has been shown both to be translocated to cell terminals and to be downregulated in the rabbit retina by laser photocoagulation.[32,35] Both translocation to bipolar cell terminals and subsequent downregulation are known to be associated with an activation of PKCα,[65] and this activation is known to be associated with injury paradigms in the retina.[66–68] Since PKCα plays a central role in cellular signal transduction and modulation of neurotransmitter release,[69] its activation is of interest to retinal functioning in general.[69,70] The data presented in the current study indicate that there was a partial translocation of PKCα to the bipolar cell terminals subsequent to lasing, but this effect was detected only in the irradiated zone and was far less obvious than previously described.[32,35] Moreover, there was no evidence of a retina-wide downregulation of PKCα. Again, though, the laser settings used in the previous studies were significantly higher than in the present study, ranging from 120 to 700 mW,[32,35] which is likely the reason that the results demonstrated a greater effect on PKCα here. As rod bipolar cells receive electrical signals from rods, which are known to be killed in the current model, it is likely that an activation of PKCα would result from the loss of synaptic input to these cells. It remains to be seen whether this activation alters signaling to downstream neurons such as amacrine cells and RGCs.

2RT Laser Irradiation

The 2RT laser has the same wavelength as a conventional CW photocoagulator laser, but its much shorter duration pulse (3 ns vs. 100 ms in the CW laser) theoretically allows targeting and ablation of the melanosome-containing RPE cells without any outward radiation of thermal energy to surrounding cells.[19] In practice, the likelihood of collateral damage to cells other than the RPE will still be dependent upon the energy setting of the laser. This is the case because at energy levels higher than the visible threshold, the energy applied will be sufficient to lead to the production of expanding and collapsing vapor bubbles in the targeted RPE cells that can damage neighboring photoreceptors.[71] We therefore analyzed the 2RT laser at two distinct energy settings: just above the visual effect threshold (high setting: 2RT-H) and at the subvisible threshold level used in clinical trials for DME[20] (low setting: 2RT-L). The 2RT laser, at the lower setting, has been shown to have an effectiveness for treatment of DME similar to that of the conventional CW

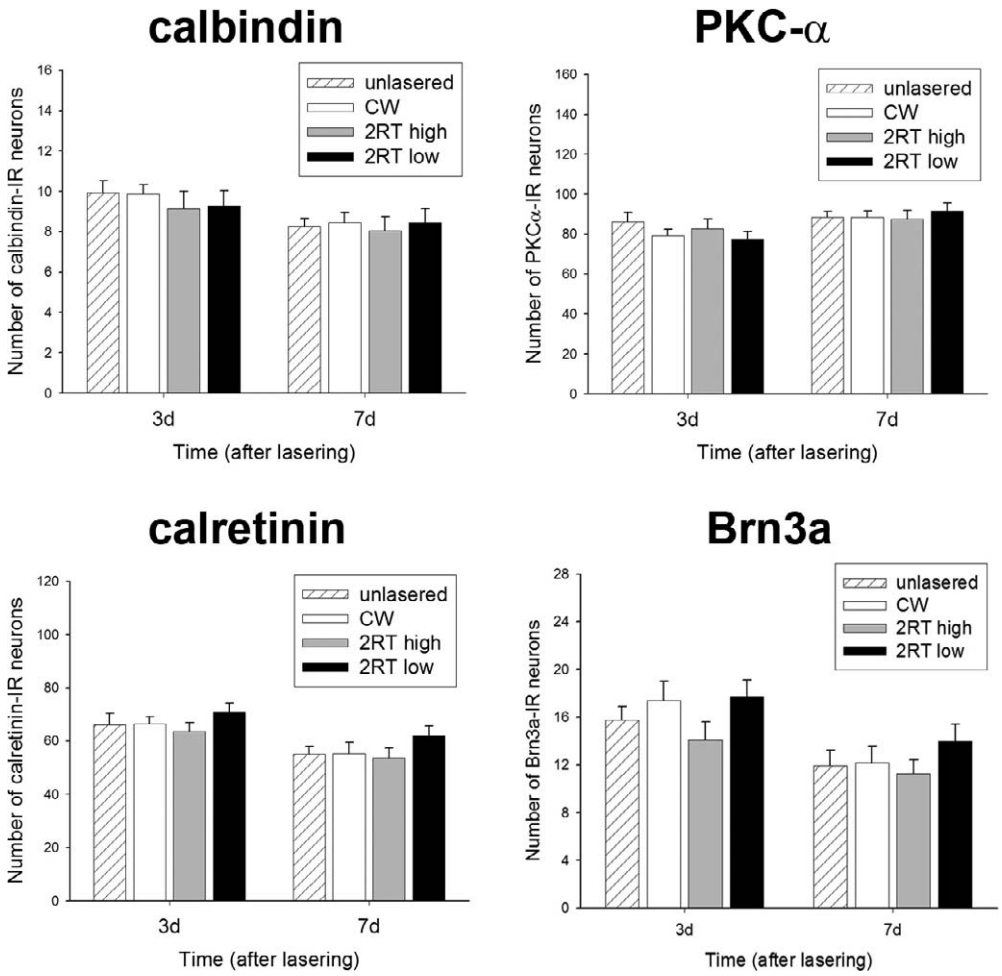

Figure 11. Quantification of numbers of horizontal cells, bipolar cells, amacrine cells, and RGCs following treatment with CW or 2RT laser, used at high and low energy settings, as determined by immunohistochemistry for calbindin, PKCα, calretinin, and Brn3a. Neurons were counted to a distance of 500 μm on each side of the central point of the irradiated region as defined in the Methods section. Data are expressed as the mean ± SEM, where $n = 15$ for each group. ANOVA revealed no significant differences between treatment groups for any of the four neuronal classes.

laser.[20] The Dark Agouti rats used in the present study featured uniform pigmentation; hence titration of the high and low energy setting between individuals was not necessary. In the clinic, variations in transparency and pigmentation between patients necessitate range finding, whereupon the high setting is first established; then the energy is titrated down for treatment purposes.

In the current study, use of the 2RT laser at either the high or low setting led to RPE loss with sparing of Bruch's membrane. In each case, as with the CW laser, RPE cells had often been replenished at the lesion site by 7 days after treatment with the 2RT laser. At the higher energy setting, however, the 2RT laser also caused significant cell loss in the outer retina. This was similar in pattern, but lower in magnitude, than the loss with the CW laser. Damage noted included apoptotic photoreceptor death and retinal structural warping and edema. A very minor number of TUNEL-positive cell nuclei were also seen after use of the 2RT laser at the low setting, but this was not consistently manifest and when present accounted for less than 5% of cells within the lased area. Neither energy setting led to detectable damage to, or death of, any inner retinal neurons. These results demonstrate two findings. First, the 2RT laser, especially when used at the energy levels defined for clinical treatment of DME patients, causes an RPE lesion that is almost entirely specific to these cells, which leaves an intact basement membrane and which is largely repaired within 7 days. This is completely in agreement with previous in vitro studies performed in pig explants using the 2RT laser,[19] as well as previous in vivo studies in rabbits performed using a microsecond line scanning laser,[58] and clearly demonstrates that the theory of selective RPE destruction for the potential clinical treatment of DME patients has a solid evidential basis. Since it is believed that stimulation of factors from RPE cells that survive treatment or lie outside of the irradiated zone underlies the beneficial wound-healing response of retinal laser treatment for DME, the ability to produce this effect with the 2RT laser alongside the almost complete sparing of adjacent photoreceptors potentially represents a useful clinical advance. This theory of retinal therapy via selective RPE destruction is also being explored in experimental and clinical trials by other researchers using different types of lasers.[18,28,59,71–76] The second finding is that despite the potential for the 2RT system to be used for DME treatment, it is clear that exceeding the visible threshold for this laser will also cause collateral damage to photoreceptors. Since the premise of this novel laser treatment is that no retinal damage will result, it is critical that operators of this laser maintain the applied energy at subvisible threshold levels. As a

final point, it should be recognized that lasers that selectively target the RPE are probably unsuited to focal use. Indeed, in the recent clinical trials of the 2RT laser, treatments were directed solely in a grid pattern, with microaneurysms not directly targeted.[20,21]

In conclusion, then, it is envisaged that the presented data, along with that from a parallel study investigating glial changes in the laser-treated rat retina,[77] will enable clinicians to better understand the effects to the retina of applying laser photocoagulation. Furthermore, this study will add to evidence that the short-pulse 2RT system, while it is as useful for treatment of DME patients as the conventional CW laser,[20] also has wider potential applications, as it does not cause the same degree of collateral tissue damage when kept at subvisible threshold energy levels. What is clear overall is that if a wound-healing response is required in the retina without the need to confine pathology to the RPE, then the conventional CW laser photocoagulator will suffice; if photoreceptor sparing is desired, then the 2RT represents an excellent alternative, possibly with the same clinical benefits for DME patients, but with a more appealing safety profile that may encourage further testing in conditions such as central serous choroidopathy and retinal vein occlusions.

Acknowledgments

The authors thank Mark Daymon and Teresa Mammone for their expert technical assistance.

References

1. Akduman L, Olk RJ. Laser photocoagulation of diabetic macular edema. *Ophthalmic Surg Lasers*. 1997;28:387–408.
2. Dorin G. Evolution of retinal laser therapy: minimum intensity photocoagulation (MIP). Can the laser heal the retina without harming it? *Semin Ophthalmol*. 2004;19:62–68.
3. Graham CE, Binz N, Shen WY, Constable IJ, Rakoczy EP. Laser photocoagulation: ocular research and therapy in diabetic retinopathy. *Adv Exp Med Biol*. 2006;572:195–200.
4. Photocoagulation for diabetic macular edema. Early Treatment Diabetic Retinopathy Study report number 1. Early Treatment Diabetic Retinopathy Study research group. *Arch Ophthalmol*. 1985;103:1796–1806.
5. Photocoagulation for diabetic macular edema: Early Treatment Diabetic Retinopathy Study report no. 4. The Early Treatment Diabetic Retinopathy Study Research Group. *Int Ophthalmol Clin*. 1987;27:265–272.
6. Goyal S, Lavalley M, Subramanian ML. Meta-analysis and review on the effect of bevacizumab in diabetic macular edema. *Graefe's Arch Clin Exp Ophthalmol*. 2011;249:15–27.
7. Lim JW, Lee HK, Shin MC. Comparison of intravitreal bevacizumab alone or combined with triamcinolone versus triamcinolone in diabetic macular edema: a randomized clinical trial. *Ophthalmologica*. 2012;227:100–106.
8. Soheilian M, Garfami KH, Ramezani A, Yaseri M, Peyman GA. Two-year results of a randomized trial of intravitreal bevacizumab alone or combined with triamcinolone versus laser in diabetic macular edema. *Retina*. 2012;32:314–321.
9. Sander B, Larsen M, Engler C, Moldow B, Lund-Andersen H. Diabetic macular oedema: the effect of photocoagulation on fluorescein transport across the blood-retinal barrier. *Br J Ophthalmol*. 2002;86:1139–1142.
10. Wallow IH. Repair of the pigment epithelial barrier following photocoagulation. *Arch Ophthalmol*. 1984;102:126–135.
11. Brancato R, Pratesi R, Leoni G, Trabucchi G, Vanni U. Histopathology of diode and argon laser lesions in rabbit retina. A comparative study. *Invest Ophthalmol Vis Sci*. 1989; 30:1504–1510.
12. Lovestam-Adrian M, Agardh E. Photocoagulation of diabetic macular oedema—complications and visual outcome. *Acta Ophthalmol Scand*. 2000;78:667–671.
13. Luttrull JK, Dorin G. Subthreshold diode micropulse laser photocoagulation (SDM) as invisible retinal phototherapy for diabetic macular edema: a review. *Curr Diabetes Rev*. 2012;8: 274–284.
14. Akduman L, Olk RJ. Diode laser (810 nm) versus argon green (514 nm) modified grid photocoagulation for diffuse diabetic macular edema. *Ophthalmology*. 1997;104:1433–1441.
15. Jain A, Blumenkranz MS, Paulus Y, et al. Effect of pulse duration on size and character of the lesion in retinal photocoagulation. *Arch Ophthalmol*. 2008;126:78–85.
16. Lavinsky D, Cardillo JA, Melo LA Jr, Dare A, Farah ME, Belfort R Jr. Randomized clinical trial evaluating mETDRS versus normal or high-density micropulse photocoagulation for diabetic macular edema. *Invest Ophthalmol Vis Sci*. 2011;52:4314–4323.
17. Luttrull JK, Musch DC, Mainster MA. Subthreshold diode micropulse photocoagulation for the treatment of clinically significant diabetic macular oedema. *Br J Ophthalmol*. 2005; 89:74–80.
18. Roider J, Liew SH, Klatt C, et al. Selective retina therapy (SRT) for clinically significant diabetic macular edema. *Graefes Arch Clin Exp Ophthalmol*. 2010;248:1263–1272.
19. Wood JP, Plunkett M, Previn V, Chidlow G, Casson RJ. Nanosecond pulse lasers for retinal applications. *Lasers Surg Med*. 2011;43:499–510.
20. Casson RJ, Raymond G, Newland HS, Gilhotra JS, Gray TL. Pilot randomized trial of a nanopulse retinal laser versus conventional photocoagulation for the treatment of diabetic macular oedema. *Clin Exp Ophthalmol*. 2012;40:604–610.
21. Pelosini L, Hamilton R, Mohamed M, Hamilton AP, Marshall J. Retina rejuvenation therapy for diabetic macular edema: a pilot study. *Retina*. 2013;33:548–558.
22. Vujosevic S, Bottega E, Casciano M, Pilotto E, Convento E, Midena E. Microperimetry and fundus autofluorescence in diabetic macular edema: subthreshold micropulse diode laser versus modified early treatment diabetic retinopathy study laser photocoagulation. *Retina*. 2010;30:908–916.
23. Belokopytov M, Belkin M, Dubinsky G, Epstein Y, Rosner M. Development and recovery of laser-induced retinal lesion in rats. *Retina*. 2010;30:662–670.
24. Ben-Shlomo G, Belokopytov M, Rosner M, et al. Functional deficits resulting from laser-induced damage in the rat retina. *Lasers Surg Med*. 2006;38:689–694.
25. Marshall J. Thermal and mechanical mechanisms in laser damage to the retina. *Invest Ophthalmol*. 1970;9:97–115.
26. Marshall J, Hamilton AM, Bird AC. Histopathology of ruby and argon laser lesions in monkey and human retina. A comparative study. *Br J Ophthalmol*. 1975;59:610–630.
27. Paulus YM, Jain A, Gariano RF, et al. Healing of retinal photocoagulation lesions. *Invest Ophthalmol Vis Sci*. 2008;49: 5540–5545.
28. Roider J, Michaud NA, Flotte TJ, Birngruber R. Response of the retinal pigment epithelium to selective photocoagulation. *Arch Ophthalmol*. 1992;110:1786–1792.
29. Rosner M, Solberg Y, Turetz J, Belkin M. Neuroprotective therapy for argon-laser induced retinal injury. *Exp Eye Res*. 1997;65:485–495.
30. Vogel A, Capon MR, Asiyo-Vogel MN, Birngruber R. Intraocular photodisruption with picosecond and nanosecond laser pulses: tissue effects in cornea, lens, and retina. *Invest Ophthalmol Vis Sci*. 1994;35:3032–3044.
31. Yu PK, Cringle SJ, McAllister IL, Yu DY. Low power laser treatment of the retina ameliorates neovascularisation in a transgenic mouse model of retinal neovascularisation. *Exp Eye Res*. 2009;89:791–800.

32. Ghosh F, Gjorloff K. Protein kinase C expression in the rabbit retina after laser photocoagulation. *Graefes Arch Clin Exp Ophthalmol*. 2005;243:803–810.
33. Humphrey MF, Moore SR. Microglial responses to focal lesions of the rabbit retina: correlation with neural and macroglial reactions. *Glia*. 1996;16:325–341.
34. Ritenour RJ, Kozousek V, Chauhan BC. The effect of panretinal photocoagulation for diabetic retinopathy on retinal nerve fibre layer thickness and optic disc topography. *Br J Ophthalmol*. 2009;93:838–839.
35. Wallenten KG, Malmsjo M, Andreasson S, Wackenfors A, Johansson K, Ghosh F. Retinal function and PKC alpha expression after focal laser photocoagulation. *Graefes Arch Clin Exp Ophthalmol*. 2007;245:1815–1824.
36. Wilson AS, Hobbs BG, Shen WY, et al. Argon laser photocoagulation-induced modification of gene expression in the retina. *Invest Ophthalmol Vis Sci*. 2003;44:1426–1434.
37. Chidlow G, Daymon M, Wood JP, Casson RJ. Localization of a wide-ranging panel of antigens in the rat retina by immunohistochemistry: comparison of Davidson's solution and formalin as fixatives. *J Histochem Cytochem*. 2011;59:884–898.
38. Chidlow G, Ebneter A, Wood JP, Casson RJ. The optic nerve head is the site of axonal transport disruption, axonal cytoskeleton damage and putative axonal regeneration failure in a rat model of glaucoma. *Acta Neuropathol*. 2011;121:737–751.
39. Chidlow G, Wood JP, Sarvestani G, Manavis J, Casson RJ. Evaluation of Fluoro-Jade C as a marker of degenerating neurons in the rat retina and optic nerve. *Exp Eye Res*. 2009;88:426–437.
40. Wood JP, Chidlow G, Graham M, Osborne NN. Energy substrate requirements for survival of rat retinal cells in culture: the importance of glucose and monocarboxylates. *J Neurochem*. 2005;93:686–697.
41. Goldring JP. Protein quantification methods to determine protein concentration prior to electrophoresis. *Methods Mol Biol*. 2012;869:29–35.
42. von Leithner PL, Ciurtin C, Jeffery G. Microscopic mammalian retinal pigment epithelium lesions induce widespread proliferation with differences in magnitude between center and periphery. *Mol Vis*. 2010;16:570–581.
43. Li R, Maminishkis A, Wang FE, Miller SS. PDGF-C and -D induced proliferation/migration of human RPE is abolished by inflammatory cytokines. *Invest Ophthalmol Vis Sci*. 2007;48:5722–5732.
44. Zhu J, Wang YS, Zhang J, et al. Focal adhesion kinase signaling pathway participates in the formation of choroidal neovascularization and regulates the proliferation and migration of choroidal microvascular endothelial cells by acting through HIF-1 and VEGF expression in RPE cells. *Exp Eye Res*. 2009;88:910–918.
45. Pons M, Marin-Castano ME. Nicotine increases the VEGF/PEDF ratio in retinal pigment epithelium: a possible mechanism for CNV in passive smokers with AMD. *Invest Ophthalmol Vis Sci*. 2011;52:3842–3853.
46. Sonoda S, Sreekumar PG, Kase S, et al. Attainment of polarity promotes growth factor secretion by retinal pigment epithelial cells: relevance to age-related macular degeneration. *Aging (Albany NY)*. 2010;2:28–42.
47. Flaxel C, Bradle J, Acott T, Samples JR. Retinal pigment epithelium produces matrix metalloproteinases after laser treatment. *Retina*. 2007;27:629–634.
48. Jennings PE, MacEwen CJ, Fallon TJ, Scott N, Haining WM, Belch JJ. Oxidative effects of laser photocoagulation. *Free Radic Biol Med*. 1991;11:327–330.
49. Matsumoto M, Yoshimura N, Honda Y. Increased production of transforming growth factor-beta 2 from cultured human retinal pigment epithelial cells by photocoagulation. *Invest Ophthalmol Vis Sci*. 1994;35:4245–4252.
50. Ogata N, Tombran-Tink J, Jo N, Mrazek D, Matsumura M. Upregulation of pigment epithelium-derived factor after laser photocoagulation. *Am J Ophthalmol*. 2001;132:427–429.
51. Starita C, Hussain AA, Marshall J. Decreasing hydraulic conductivity of Bruch's membrane: relevance to photoreceptor survival and lipofuscinoses. *Am J Med Genet*. 1995;57:235–237.
52. Starita C, Hussain AA, Pagliarini S, Marshall J. Hydrodynamics of ageing Bruch's membrane: implications for macular disease. *Exp Eye Res*. 1996;62:565–572.
53. Yoshimura N, Matsumoto M, Shimizu H, Mandai M, Hata Y, Ishibashi T. Photocoagulated human retinal pigment epithelial cells produce an inhibitor of vascular endothelial cell proliferation. *Invest Ophthalmol Vis Sci*. 1995;36:1686–1691.
54. Delori FC, Goger DG, Dorey CK. Age-related accumulation and spatial distribution of lipofuscin in RPE of normal subjects. *Invest Ophthalmol Vis Sci*. 2001;42:1855–1866.
55. Bresnick GH. Diabetic maculopathy. A critical review highlighting diffuse macular edema. *Ophthalmology*. 1983;90:1301–1317.
56. Machalinska A, Klos P, Baumert B, et al. Stem cells are mobilized from the bone marrow into the peripheral circulation in response to retinal pigment epithelium damage—a pathophysiological attempt to induce endogenous regeneration. *Curr Eye Res*. 2011;36:663–672.
57. Birngruber R, Gabel VP, Hillenkamp F. Experimental studies of laser thermal retinal injury. *Health Phys*. 1983;44:519–531.
58. Paulus YM, Jain A, Nomoto H, et al. Selective retinal therapy with microsecond exposures using a continuous line scanning laser. *Retina*. 2011;31:380–388.
59. Roider J, Hillenkamp F, Flotte T, Birngruber R. Microphotocoagulation: selective effects of repetitive short laser pulses. *Proc Natl Acad Sci U S A*. 1993;90:8643–8647.
60. Pearson AR, Tanner V, Keightley SJ, Casswell AG. What effect does laser photocoagulation have on driving visual fields in diabetics? *Eye (Lond)*. 1998;12(pt 1):64–68.
61. Venkatesh P, Ramanjulu R, Azad R, Vohra R, Garg S. Subthreshold micropulse diode laser and double frequency neodymium: YAG laser in treatment of diabetic macular edema: a prospective, randomized study using multifocal electroretinography. *Photomed Laser Surg*. 2011;29:727–733.
62. Busch EM, Gorgels TG, Van Norren D. Filling-in after focal loss of photoreceptors in rat retina. *Exp Eye Res*. 1999;68:485–492.
63. Badea TC, Cahill H, Ecker J, Hattar S, Nathans J. Distinct roles of transcription factors brn3a and brn3b in controlling the development, morphology, and function of retinal ganglion cells. *Neuron*. 2009;61:852–864.
64. Prince JH. *The Rabbit in Eye Research*. Springfield, IL: C.C. Thomas; 1964.
65. Osborne NN, Broyden NJ, Barnett NL, Morris NJ. Protein kinase C (alpha and beta) immunoreactivity in rabbit and rat retina: effect of phorbol esters and transmitter agonists on immunoreactivity and the translocation of the enzyme from cytosolic to membrane compartments. *J Neurochem*. 1991;57:594–604.
66. Osborne NN, Barnett NL. An intraocular injection of kainate induces expression of c-fos-like protein and activation of protein kinase C (alpha) in specific rabbit retinal neurones. *Brain Res Mol Brain Res*. 1992;15:108–112.
67. Osborne NN, McCord RJ, Wood J. The effect of kainate on protein kinase C, GABA, and the uptake of serotonin in the rabbit retina in vivo. *Neurochem Res*. 1995;20:635–641.
68. Osborne NN, Wood J, Muller A. The influence of experimental ischaemia on protein kinase C and the GABAergic system in the rabbit retina. *Neuropharmacology*. 1995;34:1279–1288.

69. Nishizuka Y. Protein kinase C and lipid signaling for sustained cellular responses. *FASEB J*. 1995;9:484–496.
70. Wood JPM, McCord RJ, Osborne NN. Retinal protein kinase C. *Neurochem Int*. 1997;30:119–136.
71. Brinkmann R, Huttmann G, Rogener J, Roider J, Birngruber R, Lin CP. Origin of retinal pigment epithelium cell damage by pulsed laser irradiance in the nanosecond to microsecond time regimen. *Lasers Surg Med*. 2000;27:451–464.
72. Brinkmann R, Koop N, Ozdemir M, et al. Targeting of the retinal pigment epithelium (RPE) by means of a rapidly scanned continuous wave (CW) laser beam. *Lasers Surg Med*. 2003;32:252–264.
73. Brinkmann R, Roider J, Birngruber R. Selective retina therapy (SRT): a review on methods, techniques, preclinical and first clinical results. *Bull Soc Belge Ophtalmol*. 2006;51–69.
74. Framme C, Alt C, Schnell S, Sherwood M, Brinkmann R, Lin CP. Selective targeting of the retinal pigment epithelium in rabbit eyes with a scanning laser beam. *Invest Ophthalmol Vis Sci*. 2007;48:1782–1792.
75. Prahs P, Walter A, Regler R, et al. Selective retina therapy (SRT) in patients with geographic atrophy due to age-related macular degeneration. *Graefes Arch Clin Exp Ophthalmol*. 2010;248:651–658.
76. Roider J, Brinkmann R, Wirbelauer C, Laqua H, Birngruber R. Retinal sparing by selective retinal pigment epithelial photocoagulation. *Arch Ophthalmol*. 1999;117:1028–1034.
77. Chidlow G, Shibeeb O, Plunkett M, Casson RJ, Wood JPM. Glial cell and inflammatory responses to retinal laser treatment: comparison of a conventional photocoagulator and a novel, 3-nanosecond pulse laser. *Invest Ophthalmol Vis Sci*. 2013;54:2319–2332.